Analysis of liquid-lubricated herringbone grooved journal bearings

T.S. Lee, Y.G. Liu and S.H. Winoto
Department of Mechanical Engineering, National University of Singapore, Singapore

Received August 2002
Revised June 2003
Accepted July 2003

Keywords *Cavitation, Fluid dynamics, Lubricants, Lubricating systems*

Abstract *Numerical studies are carried out to investigate the liquid-lubricated herringbone-grooved journal bearings (HGJBs) performance (such as the pressure and cavitation distribution, load capacity and attitude angle, stability, etc.). Symmetrical and non-symmetrical HGJBs are studied, respectively, and the herringbone grooves' influence on the stability of HGJBs is analyzed carefully. It was found that the maximum pressure and load capacity increase with the increase of eccentricity ratio while the attitude angle decreases with the increase of eccentricity ratio. The cavitation may occur in the fluid film of journal bearings while the eccentricity ratio increases to some critical value. The area of cavitated region increases with the increase of the eccentricity ratio. For non-symmetrical HGJBs, the pressure and cavitation distribution is asymmetrical oo.*

Nomenclature

h_g, H_g = groove depth
$\beta\ \bar{\beta}$ = bulk modulus, dimensionless $\beta(\bar{\beta} = (\beta/\omega\mu)(c/R)^2)$
c, R = radial clearance, bearing radius
L_1, L_2 = grooves' length of part one, part two
L = length of journal bearing) $(L = L_1 + L_2)$
L/D = ratio of length to diameter $(D = 2R)$
$h, \bar{h}$ = film thickness, dimensionless film thicknes (h/c)
w_g, w_r = groove width, groove ridge width
$P, \bar{P}$ = film pressure, dimensionless P, $\bar{P} = (P/\omega\mu)(c/R)^2$
$P_B, \bar{P}_s$ = ambient pressure, dimensionless ambient pressure
$P_C, \bar{P}_c$ = cavitation pressure, dimensionless cavitation pressure
$W, \bar{W}$ = load capacity, dimensionless $W\ (\bar{W} = (W/\omega\mu R^2)(c/R)^2)$
ϕ, α = attitude angle, groove angle
μ, ρ = fluid viscosity, fluid density
ρ_c = fluid density at cavitation pressure
ω, U = angular rotation speed, rotational speed $(\omega \cdot R)$
e, ε = eccentricity, eccentricity ratio (e/c) (or epsn)
$t, \bar{t}$ = time, dimensionless time (ωt)
x = coordinate in circumference direction
$\bar{x}$ = dimensionless x, $(\bar{x} = x/2\pi R)$
y = coordinate in fluid film thickness
z = coordinate in axial direction
$\bar{z}$ = dimensionless of $z\ (\bar{z} = z/L)$
ξ = coordinate axis in the transformed plane
η = coordinate axis in the transformed plane
ϕ = circumferential coordinate
θ = density ratio (ρ/ρ_c)
g = switch function

International Journal of Numerical Methods for Heat & Fluid Flow
Vol. 14 No. 3, 2004
pp. 341-365

0961-5539
DOI 10.1108/09615530410517995

1. Introduction

With the trend of miniaturization and high-speed requirement in modern industry, much attention has been given to the use of fluid dynamic bearings, especially the herringbone-grooved journal bearings (HGJBs). For example, in computer industry, after many research works, HGJBs are used in the spindle motor of hard disk drive (HDD) to replace the traditional ball bearings. Compared with the traditional ball bearings, the HGJBs have considerably lower noise level, relatively higher stiffness and better stability, even worked under high rotational speeds.

For the fluid dynamic bearings, with the increase of the eccentricity ratio, the cavitation may occur in the fluid film. When cavitation collapses, cavitation erosion may occur and cause cavitation damage to the bearings (Dowson and Taylor, 1979). Thus, for the numerical study of fluid dynamic bearings, how to treat the cavitation boundary condition is very important. Various cavitation boundary conditions have been proposed by earlier researchers, such as the Sommerfeld conditions, Reynolds conditions and JFO (Jakobsson-Floberg-Olsson, named after Jakobsson and Floberg (1957) and Olsson (1965)) theory, etc. Among them, the JFO theory is regarded as one of the best theories that account for the flow physics of a fluid film: the rupture and the reformation. According to this theory, the fluid film in journal bearings can be divided into two zones: the full-film zone and the cavitated zone. However, the mass conservation is preserved in the whole fluid film, not only in the full-film zones, but also in the cavitated zones and in the interfaces between them. Many case studies show that, when this theory is applied to the numerical simulation of the journal bearings, the predicted results match the experimental data very well.

Based on the JFO theory, Elrod and Adams (1974) derived a generalized form of Reynolds' differential equation in which the complexities of locating film rupture and reformation boundaries are avoided as this scheme automatically predicts cavitation regions and preserves mass continuity within all the fluid film for the liquid-lubricated bearings. Later, Elrod (1981) modified the finite definite difference portion of the scheme, and presented a much better cavitation algorithm: the so-called Elrod's cavitation algorithm. This computational scheme automatically implements the JFO theory, then mass conservation is preserved in the whole fluid film.

Studies on the HGJBs were started very early: in 1965, Hirs did some research on HGJBs by experimental study and theoretical analysis. Even at present, his experimental findings are referred to by many researchers. However, in the earlier studies of HGJBs, the cavitation is often neglected. Recently, Elrod's cavitation algorithm or its modified version was introduced to study journal bearings, especially HGJBs, a lot of progresses have been made. Vijayaraghavan and Keith (1990a) extended the work of Elrod (1981) and

proved that an approximate factorization technique in conjunction with Newton's iteration method for time accurate solutions can apply to both steady and unsteady state conditions. The grid transformation and grid adaptation techniques, presented by Vijayaraghavan and Keith (1990b) was stated to be more suitable for more complicated problems and for saving the computational efforts.

Jang and Chang (2000) analyzed the performance of a HGJB in the spindle motor of a computer HDD including the effects of cavitation. In their paper, the Reynolds equation is solved using the finite volume method. The performance (such as the load capacity, the attitude angle, the bearing torque and the cavitation ratio of the fluid film, etc.) is studied for the symmetrical HGJBs.

Wan *et al.* (2002) presented a numerical model to describe better the cavitated fluid flow phenomena in the liquid lubricated HGJBs. By using an effective "following the groove" grid transformation method, the singularity at the groove edges is avoided. The cavitation footprint of the HGJBs is analyzed, for the symmetrical and asymmetrical groove patterns, respectively.

In this work, using the modified Elrod's algorithm, the liquid-lubricated HGJBs' performance is analyzed. By incorporating the JFO theory and Elrod's algorithm, the modified Reynolds equation is used as the governing equation. To capture all of the groove boundaries, the groove-shape-fitted grids are constructed (Figures 1 and 2) and a coordinate transformation method is used. After the modified Reynolds equation is transformed into the rectangular computational region, the finite difference discretizing method is used to discrete the equation and the alternating direction implicit (ADI) method is used to solve the equation. Based on this methodology, the plain journal bearings (plain JBs), the symmetrical and non-symmetrical HGJBs are analyzed, respectively.

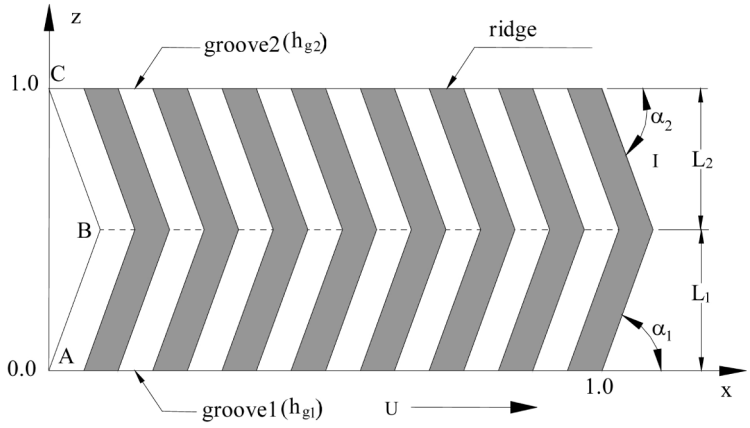

Figure 1.
Unwrapped geometry and some parameters of a HGJBs

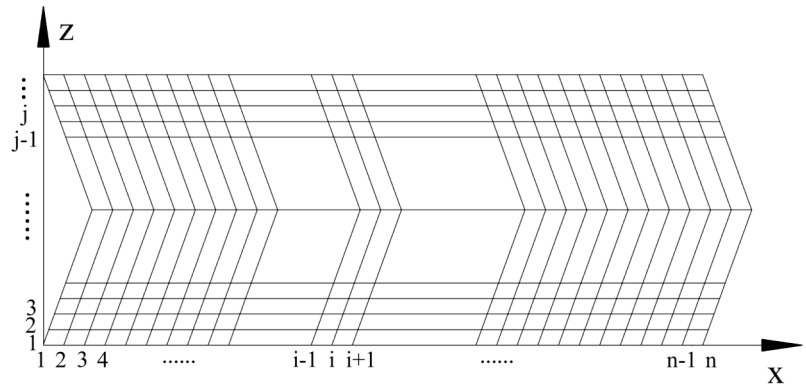

Figure 2.
Groove-shape-fitted grids system for HGJBs

2. Methodology

2.1 Governing equations

In the numerical studies of HGJBs, the external mass forces and inertial forces are often neglected. For the laminar flow of Newtonian lubricants, the two-dimensional transient form of Reynolds equation can be written as:

$$\frac{\partial \rho h}{\partial t} + \frac{\partial}{\partial x}\left(\frac{\rho h U}{2} - \frac{\rho h^3}{12\mu}\frac{\partial P}{\partial x}\right) + \frac{\partial}{\partial z}\left(-\frac{\rho h^3}{12\mu}\frac{\partial P}{\partial z}\right) = 0 \tag{1}$$

in which the compressibility effect of the fluid is considered.

According to the definition of the bulk modulus β, the fluid's density field is related to the pressure field of the fluid film by:

$$\beta = \rho\, \partial P / \partial \rho \tag{2}$$

To satisfy the JFO theory, in which the pressure throughout the cavitated zone is taken as a constant, the switch function g and the non-dimensional density variable θ are introduced. Then equation (2) becomes:

$$g\beta = \rho\frac{\partial P}{\partial \rho} = \theta\frac{\partial P}{\partial \theta} \tag{3}$$

where $\theta = \rho/\rho_c$, and in cavitated region: $\theta < 1, g = 0$ whereas in the full film region, $\theta \geq 1, g = 1$. From equation (3), we obtain:

$$P = P_c + g\beta \ln \theta \tag{4}$$

Using equations (3) and (4), equation (1) can be rewritten as:

$$\frac{\partial \rho_c h\theta}{\partial t} + \frac{\partial}{\partial x}\left(\frac{\rho_c h U}{2}\theta - \frac{\rho_c \beta h^3 g}{12\mu}\frac{\partial \theta}{\partial x}\right) + \frac{\partial}{\partial z}\left(-\frac{\rho_c \beta h^3 g}{12\mu}\frac{\partial \theta}{\partial z}\right) = 0 \tag{5}$$

The non-dimensional form of this equation is:

$$\frac{\partial(\theta\bar{h})}{\partial t}+\frac{1}{4\pi}\frac{\partial(\theta\bar{h})}{\partial\bar{x}}=\frac{\bar{\beta}}{48\pi^2}\frac{\partial}{\partial\bar{x}}\left(\bar{h}^3g\frac{\partial\theta}{\partial\bar{x}}\right)+\frac{\bar{\beta}}{48(L/D)^2}\frac{\partial}{\partial\bar{z}}\left(\bar{h}^3g\frac{\partial\theta}{\partial\bar{z}}\right) \quad (6)$$

2.2 Coordinate transformation

To model the shape of the herringbone grooves accurately, the groove-shape-fitted grids are constructed: the grids are arranged along the slant grooves in the (x-z) plane (Figures 1 and 2). Then to simplify the computation, a coordinate transformation method – from the physical region (x-z) to the rectangular computational region (ξ-η) is used (Shu *et al.*, 2000). The x-direction is taken as the ξ-direction while the groove direction is taken as the η-direction.

$$f_x=\frac{\partial f}{\partial x}=\xi_x\frac{\partial f}{\partial\xi}+\eta_x\frac{\partial f}{\partial\eta} \quad (7)$$

$$f_z=\frac{\partial f}{\partial z}=\xi_z\frac{\partial f}{\partial\xi}+\eta_z\frac{\partial f}{\partial\eta} \quad (8)$$

$$\xi_x=J^{-1}z_\eta;\quad \eta_x=-J^{-1}z_\xi;\quad \xi_z=-J^{-1}x_\eta;\quad \eta_z=J^{-1}x_\xi \quad (9)$$

where $J=x_\xi z_\eta-x_\eta z_\xi$ is the Jacobian of the transformation.

Hence, for steady state, the non-dimensional Reynolds' equation in the computational domain can be obtained as:

$$\begin{aligned}\frac{\partial\theta}{\partial\bar{t}}=&-\frac{1}{4\pi}\frac{\partial\bar{h}}{\partial\xi}\frac{\theta}{\bar{h}}-\frac{1}{4\pi}\frac{\partial\theta}{\partial\xi}+\frac{\partial g(\theta-1)}{\partial\xi}\left[\frac{\beta}{48\pi^2}3\bar{h}\frac{\partial\bar{h}}{\partial\xi}+\frac{\beta}{48(L/D)^2}3\bar{h}\xi_z\right.\\&\left.\left(\xi_z\frac{\partial\bar{h}}{\partial\xi}+\eta_z\frac{\partial\bar{h}}{\partial\eta}\right)\right]+\frac{\partial g(\theta-1)}{\partial\eta}\left[\frac{\beta}{48(L/D)^2}3\bar{h}\left(\xi_z\frac{\partial\bar{h}}{\partial\xi}+\eta_z\frac{\partial\bar{h}}{\partial\eta}\right)\right]\\&+\frac{\partial^2g(\theta-1)}{\partial\xi^2}\left[\frac{\beta}{48\pi^2}\bar{h}^2+\frac{\beta}{48(L/D)^2}\bar{h}^2\xi_z^2\right]\\&+\frac{\beta\bar{h}^2}{48(L/D)^2}\left[\xi_z\frac{\partial}{\partial\xi}\left(\frac{\partial g(\theta-1)}{\partial\eta}\right)+\frac{\partial}{\partial\eta}\left(\xi_z\frac{\partial g(\theta-1)}{\partial\xi}\right)\right]\\&+\frac{\beta\bar{h}^2}{48(L/D)^2}\frac{\partial^2g(\theta-1)}{\partial\eta^2}\end{aligned} \quad (10)$$

2.3 Load capacity and attitude angle

When the pressure and velocity fields of the fluid film are known, the load capacity W, and attitude angle ϕ can be calculated by using the following formulae:

$$W = \sqrt{F_{\varphi}^2 + F_R^2} \tag{11}$$

$$\phi = \tan^{-1}(F_{\varphi}/F_R) \tag{12}$$

where F_R is the pressure force acting along the line of centers, and F_{ϕ} is the pressure force normal to that line.

$$F_{\varphi} = \iint_S P \sin\varphi \, dx \, dz \tag{13}$$

$$F_R = \iint_S P \cos\varphi \, dx \, dz \tag{14}$$

2.4 Numerical method

As in other numerical studies on journal bearings (Jang and Chang, 2000; Wan *et al.*, 2002), the fluid film is unwrapped around the circumferential direction (Figure 1). The Reynolds equation can be solved in a two-dimensional domain. Equation (1) shows that the flow in x-direction consists of two parts. One part is due to shear flow and the other part is due to diffusion flow (pressure gradient), while the flow in the z-direction is due to diffusion flow only.

In this work, the finite difference method is used to discretize the governing equation – equation (10). For the diffusion flow terms, many symmetric numerical methods, such as central finite difference method and Galerkin finite element method, can be used. However, for the shear flow terms, because the physical information is transferred from the upstream to the downstream, it is a non-symmetrical problem in space. So, there will be some intrinsic difficulties if the symmetrical numerical methods are used to them. Conversely, the upwind scheme, in which the numerical information propagates from upstream to downstream conforming to the physical phenomenon, is very powerful to deal with the shear terms. So, in this study, the central difference method is used to discretize the pressure flow terms, and the second order upwind scheme is used to discretize the shear flow terms.

The present problem is simplified into a two-dimensional problem. Once discretization is completed, the equation is solved by using the ADI method. In this approach, each time step is split into two parts. In the first part, all rows are implicitly solved by using the available values of the variables at the previous step. In the second part, all columns are solved implicitly by using the available values of the variables obtained from the first part. A four-stage Runge-Kutta (R-K) method is also tried, but it is found that the ADI method is more efficient and stable than the R-K method. However, in our calculations, even if we use

the ADI method, some instability may occur if the time step is too large. In other words, if we choose a proper time step, the ADI method is stable.

3. Validation

Based on the equations and methodology mentioned earlier, a computational program is built up to study the performance of the journal bearings. To validate this program, two cases (Table I) are studied and the numerical results are compared with the experimental data, respectively.

First, a case of plain JB (no grooves on the surface of the shaft or bush) is introduced and the numerical results are compared with Jakobsson and Floberg's (1957) experimental data. Table I (case 1) presents the experimental operating conditions detailed by Brewe (1986). Figure 3 shows the circumferential pressure distribution at an axial location: the axial distance (ΔL) equals (1/5)D. This figure shows that the numerical results match well with the experimental data.

For HGJBs, a typical case (case 2 in Table I, detailed by Hirs (1965) and Jang and Chang (2000)) is studied and the predicted load capacity is shown in Figure 4. This figure shows that, for HGJBs, with the increase of eccentricity ratio, the load capacity will increase, just like the experimental data, which were given by Hirs (1965). Figure 4 also shows that for HGJBs, the numerical results match very well with the experimental data.

4. Studies of the pumping effect of herringbone grooves

As shown in Figure 1, there are two "legs" for each herringbone groove: AB and BC. For the convenience in analyzing the journal bearings' performance, we divide the HGJB into two parts along the line of the apexes (the dashed line in Figure 1): part I and part II. In symmetrical HGJBs, the geometric parameters in these two parts are the same. So, for symmetrical HGJBs, we have: $L_1 = L_2$,

	Case 1 (plain-JB)	Case 2 (HGJBs)
Number of grooves	0	8
c (m)	1.455×10^{-4}	6.0×10^{-6}
R (m)	0.05	0.002
L/D	4/3	1.0
ε	0.61	0.60
ω_s	-48.1(rad/s)	5,000(rpm)
β (N/m^2)	1.72×10^9	1.72×10^9
μ (N/m^2)	0.0127	0.00124
P_B (N/m^2)	0.0	0.0
P_c (N/m^2)	-72139.79	-72139.79
α (deg)	–	70.0
h_{g1}/c	0.0	1.0
h_{g2}/c	0.0	1.0
w_g/w_r	–	1.0

Table I. Geometrical dimension and operating conditions

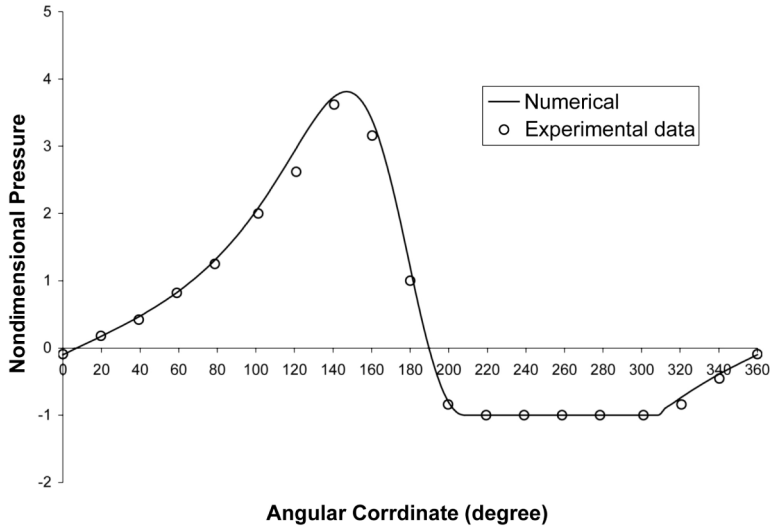

Figure 3.
Comparison of predicted pressure with experimental data

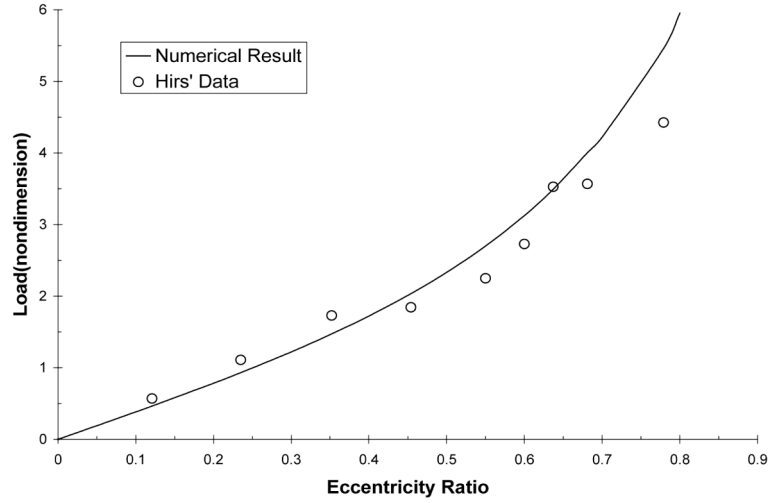

Figure 4.
Comparison of non-dimensional load capacity for HGJBs (case 2 of Table I)

$\alpha_1 = \alpha_2$, $h_{g1} = h_{g2}$. While in non-symmetrical HGJBs, one or several geometrical parameters are not the same between parts I and II. In this part of our project, a symmetrical HGJB case (case 3 in Table II) is introduced to study the herringbone grooves' pumping effect. In this case, the geometrical and operating conditions are similar to case 2 (Table I), except that the eccentricity ratio is variable. In order to compare the stability between HGJBs and plain JBs, a case of plain JB (case 4 in Table II) is introduced. The geometrical and operating conditions are similar between case 3 and case 4,

	Case 3 (HGJBs)	Case 4 (plain-JBs)
Number of grooves	8	0
c (m)	6.0×10^{-6}	6.0×10^{-6}
R (m)	0.002	0.002
L/D	1.0	1.0
ε	0.01-0.80	0.01-0.80
ω (rpm)	5,000	5,000
β (N/m^2)	1.72×10^9	1.72×10^9
μ (N/m^2)	0.00124	0.00124
h_{g1}/c	1.0	0
h_{g2}/c	1.0	0
α (°)	70	–
w_g/w_r	1.0	–
P_B (N/m^2)	0.0	0.0
P_c (N/m^2)	−72139.79	−72139.79

Table II.
Geometrical and operating conditions of journal bearings

except that in case 4, no grooves in the journal or bearing's surface (the so-called plain-JBs), while in case 3, herringbone grooves are engraved in the outside surface of the shaft or in the inside surface of the bush (the so-called HGJBs). The numerical results are shown in Figures 5-12.

4.1 The stability analysis of HGJBs and plain JBs

For rotating machinery, especially those operating at high speed, the instability is one of the main problems. There are many factors, which may cause the rotating machine's instability, such as the magnetic pulls, aerodynamic forces on turbine or compressor blades, gear impacts, etc. In journal bearings, the lubricant films themselves might originate the undesirable self-excited vibration, known as "half-frequency whirl", in which the shaft orbits around the center of the bearing at a frequency approximately equal to half of the

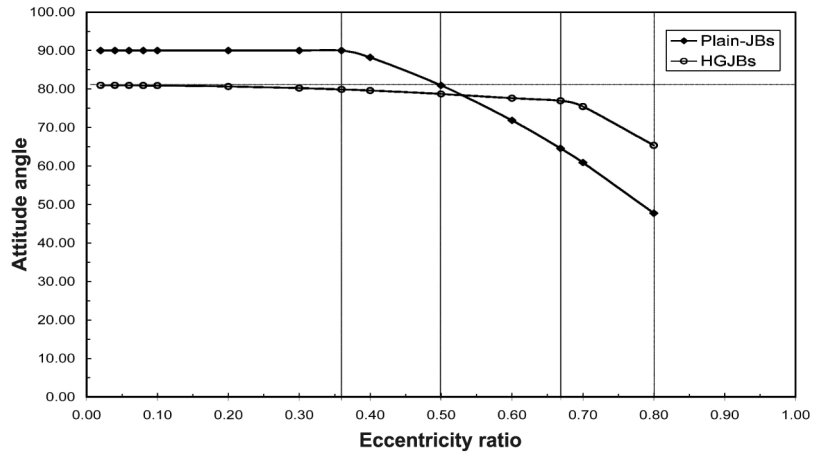

Figure 5.
Attitude angle of HGJBs and plain-JBs due to eccentricity ratio

spinning or rotational velocity of the shaft, or a little less (Fuller, 1984). In journal bearings' operation, this is one of the most serious forms of instability, which will cause destructive damage to the journal bearings. Hagg (1946) showed that when the "half-frequency whirl" occurs, the capacity of the bearing to support radial loads falls to zero, which means that F_R (the pressure

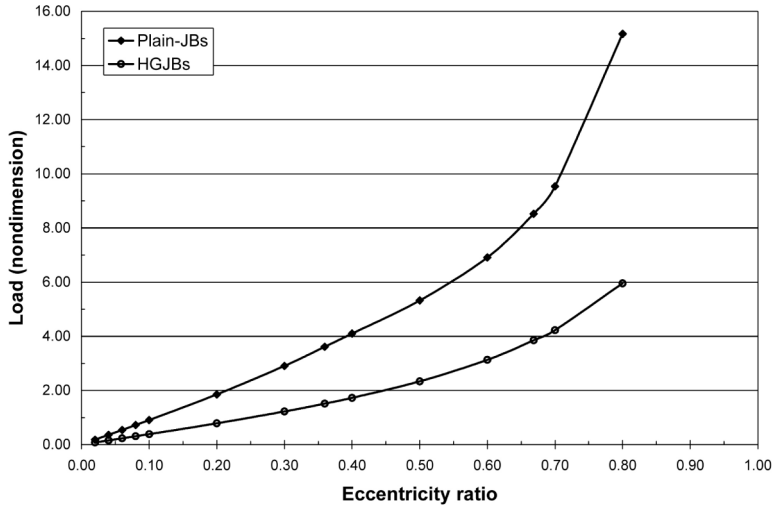

Figure 6.
Load capacity of HGJBs and plain-JBs due to eccentricity ratio

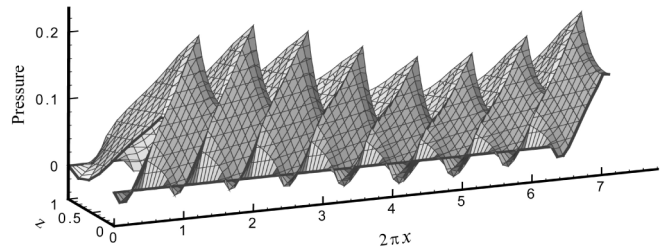

(a) For HGJBs

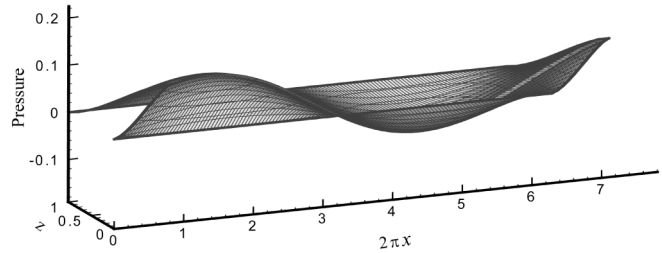

(b) For Plain-JBs

Figure 7.
Comparison of the dimensionless pressure distribution between the HGJBs and the plain JBs at different eccentricity ratios

(a) Dimensionless pressure distribution at ε =0.04

(continued)

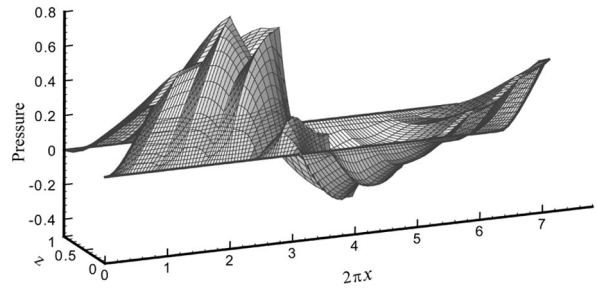

(a) For HGJBs

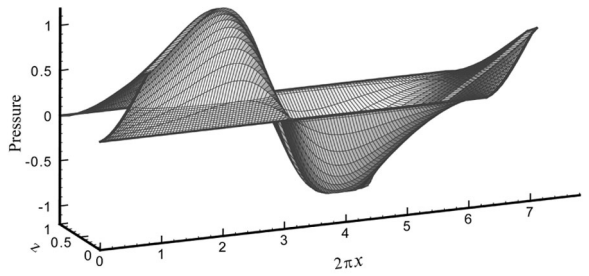

(b) For Plain-JBs

(b) Dimensionless pressure distribution at ε =0.40

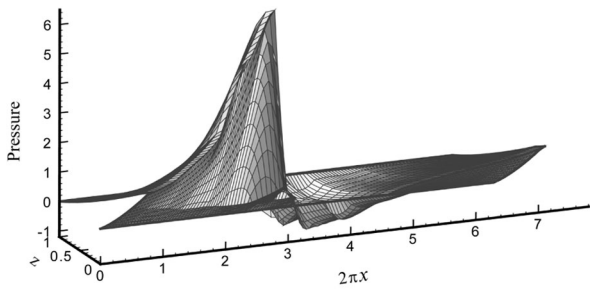

(a) For HGJBs

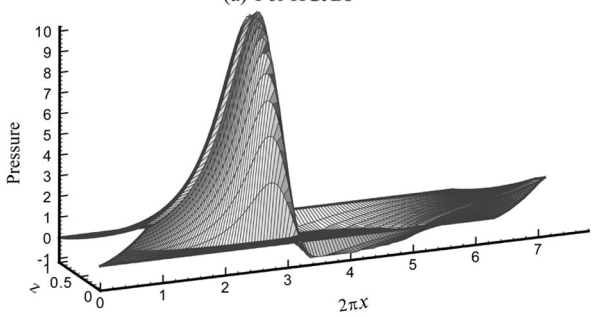

(b) For Plain-JBs

(c) Dimensionless pressure distribution at ε =0.80

Figure 7.

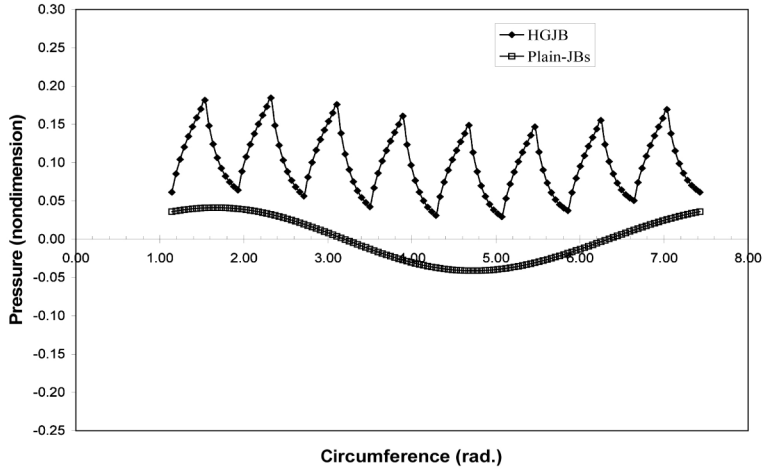

(a) Middle line's dimensionless pressure profile at ε =0.02

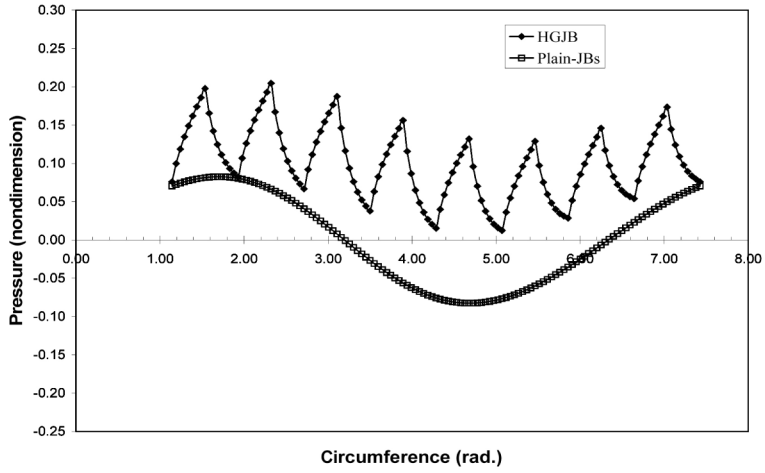

(b) Middle line's dimensionless pressure profile at ε =0.04

Figure 8.
Comparison of the dimensionless pressure (along the middle line) between the HGJBs and plain-JBs.

force acting along the line of centers, equation (14)) equals zero. Thus, if F_{φ} (the pressure force normal to the line of centers, equation (13)) does not equal zero, the attitude angle ϕ will almost equal 90° (equation (12)).

For the cases studied (case 3 and case 4 in Table II), the numerical results of attitude angle are presented in Figure 5. This figure shows that for plain JBs, the instable condition – the half-frequency whirl – will occur at small values of the eccentricity ratio (ε), now that the attitude angle is almost 90° when ε is very small ($\varepsilon \leq 0.36$ in case 3 of Table II). With the increase of ε,

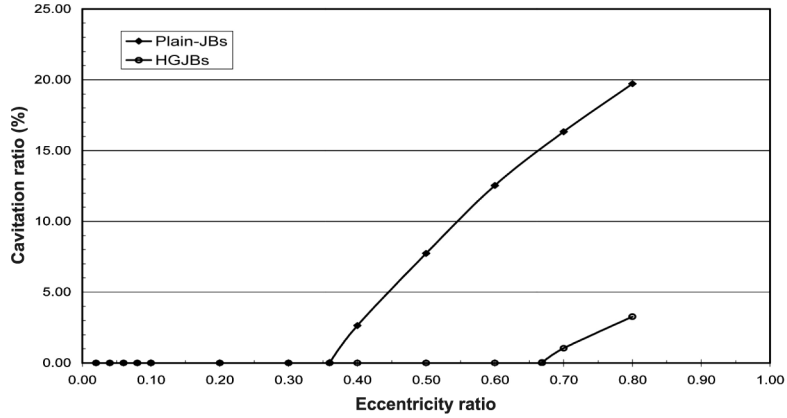

Figure 9.
Cavitation ratio of HGJBs and plain-JBs due to eccentricity ratio

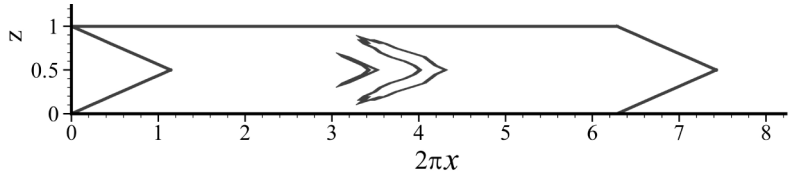

(a) Cavitation distribution for HGJBs at ε =0.80

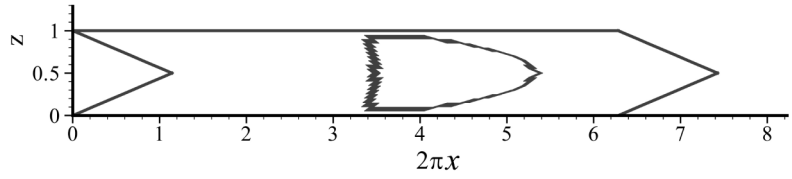

(b) Cavitation distribution for Plain-JBs at ε =0.80

Figure 10.

the attitude angle will decrease. When ε equals 0.50, the attitude angle reaches about 81°.

On the other hand, for HGJBs, Figure 5 shows that even ε is very small (for example, $\varepsilon = 0.02$), the attitude angle is about 81°, much smaller than 90°. With the increase of ε, the attitude angle also decreases. This figure shows that for HGJBs, the unstable condition – the half-frequency whirl – will never occur. This is one of the main advantages of HGJBs: compared to plain JBs, the HGJBs are much more stable.

4.2 Comparison of load capacities of HGJBs and plain JBs

The load capacities of the HGJBs and plain JBs are shown in Figure 6. For HGJBs, this figure shows that, the load capacity increases with the increase of eccentricity ratio, just like the plain-JBs, however, the variation of HGJBs is relatively small than that of the plain-JBs. Thus, in terms of load capacity, for

the light loaded journal bearings, the difference between HGJBs and plain-JBs is very small. However, for heavy loaded journal bearings, the plain JB may be better than the HGJBs, now that at the same eccentricity ratio, the plain-JBs' load capacity is bigger than that of the HGJBs.

4.3 The pressure and cavitation distribution of HGJBs and plain JBs

For the case studies (cases 3 and 4 in Table II), some of the results about the pressure and cavitation distrubution are shown in Figures 7-10. Figure 7 shows

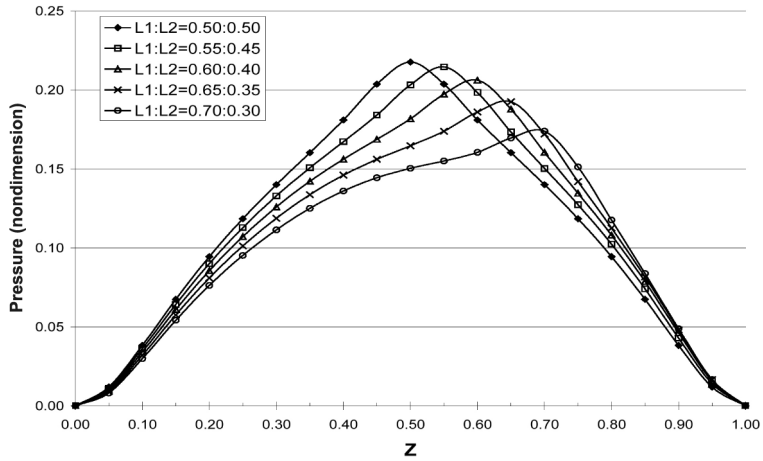

(a) Pressure distribution along grooves at $2\pi x = 0.9817$ for $\varepsilon = 0.10$

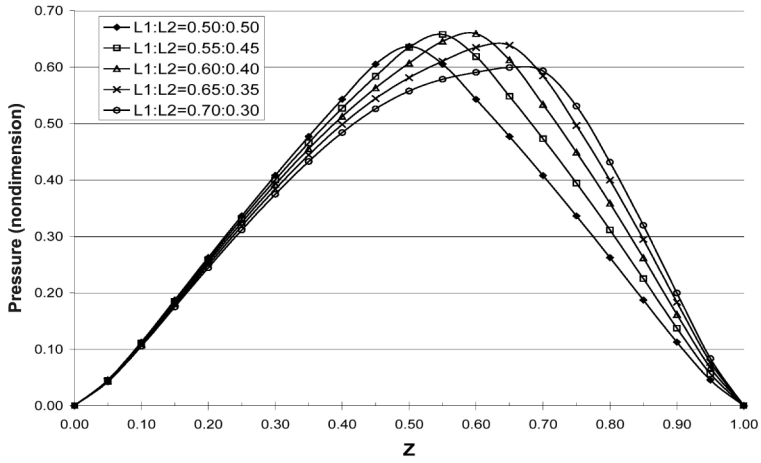

(b) Pressure distribution along grooves at $2\pi x = 0.9817$ for $\varepsilon = 0.40$

(continued)

Figure 11.
Pressure distribution (along the grooves at $2\pi x = 0.9817$ or $x = 0.15625$)

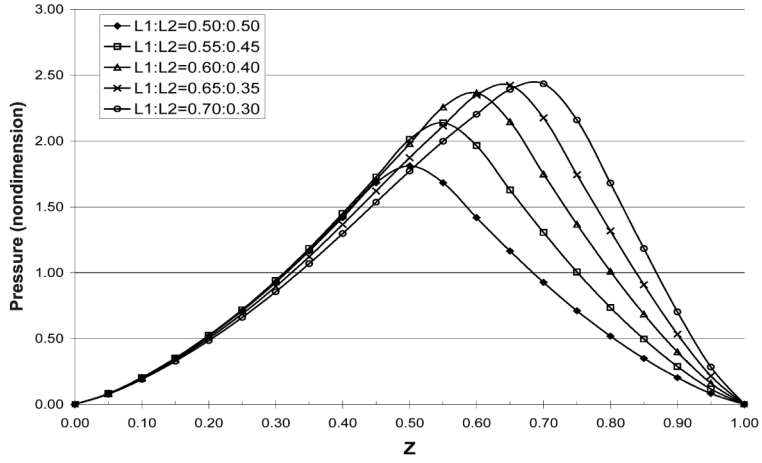

(c) Pressure distribution along grooves at $2\pi x = 0.9817$ for $\varepsilon = 0.80$

Figure 11.

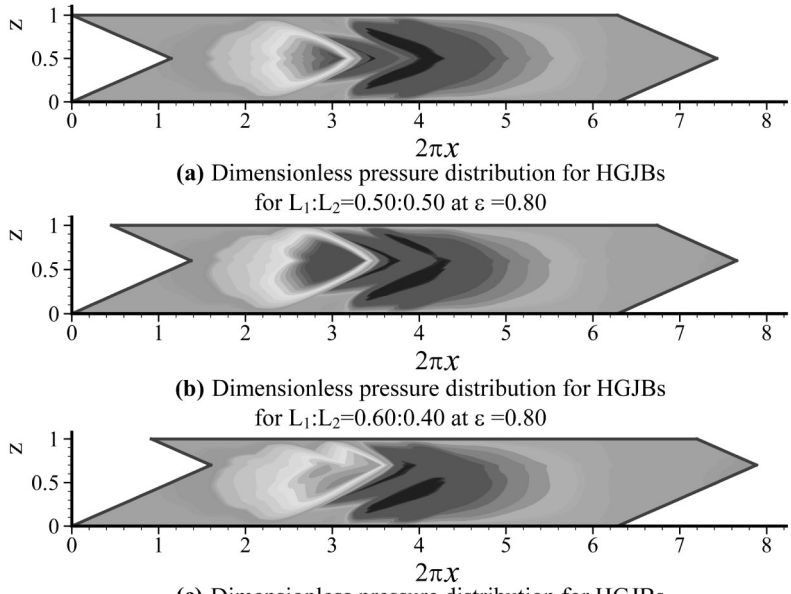

(a) Dimensionless pressure distribution for HGJBs for L_1:L_2=0.50:0.50 at $\varepsilon = 0.80$

(b) Dimensionless pressure distribution for HGJBs for L_1:L_2=0.60:0.40 at $\varepsilon = 0.80$

(c) Dimensionless pressure distribution for HGJBs for L_1:L_2=0.70:0.30 at $\varepsilon = 0.80$

Figure 12.

the dimensionless pressure distribution in the unwrapped geometrical region, while Figure 8 shows the dimensionless pressure profiles along the middle line (the dashed line in Figure 1) along the circumferential direction, for HGJBs and plain-JBs, respectively.

Figures 7 and 8 show that the pressure distribution is different between HGJBs and plain JBs, especially when the eccentricity ratio is small. This is because of herringbone grooves' pumping effect: lubricant is pumped inward the journal bearings along the herringbone grooves, thus pressure is built up along the grooves, even in the divergent region of the bearings' fluid film (the pressure is higher than the boundary pressure in the grooves), and when the eccentricity ratio tends to zero, the pressure distribution becomes periodic (Figure 8). On the other hand, for plain-JBs, no pressure is set up in the divergent region of bearings' fluid film; when the eccentricity ratio tends to zero, the pressure distribution becomes zero (unstable conditions of half-frequency whirl). This is why there is half-frequency whirl for plain JBs, but no half-frequency whirl for herringbone journal bearings, even the eccentricity ratio is very small.

As shown in Figure 7, with the increase of eccentricity ratio, the maximum pressure in the fluid film of journal bearings will increase. When the eccentricity ratio increases to some critical value, the cavitation will occur in the fluid film, even though this value is not the same between HGJBs and plain-JBs. Figures 9 and 10 compare the cavitation distribution between HGJBs and plain-JBs.

For the liquid lubricated journal bearings, inside its fluid film, the cavitation is often caused by the fall of pressure in the lubricant. However, for HGJBs, because of the herringbone grooves' pumping effect, the pressure is generated inside the grooves, even in the divergent region of the bearings' fluid film. So, inside the fluid film of HGJBs, this kind of pressure (generated due to the herringbone grooves' pumping effect) can prevent the formation of cavitation, or reduce the area of the cavitated region to some extent, as shown in Figures 9 and 10. Figure 9 shows that for plain JBs, the cavitation begins to occur in fluid film when the eccentricity ratio is about 0.36, while for HGJBs, there is no cavitation until the eccentricity ratio is higher than 0.67. Figure 10 shows that, once the cavitation occurs in the fluid film, at the same eccentricity ratio, the area of the cavitated region is different between the HGJBs and the plain-JBs: the cavitation region of HGJBs is much less than that of the plain-JBs.

4.4 Discussion

By adding herringbone grooves on the surface of journal bearings, the fluid is pumped inward the journal bearings along the grooves, then the pressure is built up along the grooves, even in the divergent region of the bearings' fluid film. Compared with the plain JBs, this kind of pressure can prevent cavitation in the fluid film and increase the journal bearings' stability. For HGJBs, when the eccentricity ratio tends to zero, the pressure distribution becomes periodic, which contributes to its stability: no "half-frequency whirl" in HGJBs. On the other side, it also decreases the corresponding maximum pressure (compared with the plain JBs) in the fluid film, and decreases the journal bearings load capacity.

5. Study the performance of non-symmetrical HGJBs

For non-symmetrical HGJBs, there are many different cases to study, now that there are so many geometrical parameters in each part (Figure 1). In this part, we will study the effect of the groove-length ratio ($L_1 : L_2 = \mathrm{AB} : \mathrm{BC}$) and the groove-depth ratio ($hg_1 : hg_2$) on the performances of the non-symmetrical HGJBs, which means that, between parts I and II (Figure 1), the groove length or groove depth may not be the same ($L_1 \neq L_2$ or $hg_1 \neq hg_2$), while others are the same. As shown in Table III, two cases are introduced, in which the geometrical and operating conditions are based on case 2 of Table I. The numerical results are presented and discussed later.

5.1 The influence of groove-length ratio on non-symmetrical HGJBs

Case 5 (Table III) was used to study the effect of groove-length ratio ($L_1 : L$) on the performance of non-symmetrical HGJBs. The numerical results are presented in Figures 11-14.

5.1.1 The pressure and cavitation distribution due to the groove-length ratio. The pressure and cavitation distribution is shown in Figures 11-13. Figure 11 shows the pressure distribution along the groove direction at $2\pi x = 0.9817$ (or $x = 0.15625$), when the eccentricity ratio is varied from 0.02 to 0.80 and the length ratio ($L_1 : L$) changes from 0.50 to 0.70 ($L_1 : L + L_2 : L = 1.0$). Figures 12 and 13 show the pressure and cavitation distribution in the unwrapped geometrical region due to different groove-length ratio when the eccentricity ratio equals 0.80.

	Case 5	Case 6
Number of grooves	8	8
c (m)	6.0×10^{-6}	6.0×10^{-6}
R (m)	0.002	0.002
L/D	1.0	1.0
ε	0.01-0.80	0.01-0.80
ω (rpm)	5,000	5,000
β (N/m^2)	1.72×10^9	1.72×10^9
μ (N/m^2)	0.00124	0.00124
L_1/L	*Variable	0.50
L_2/L	*Variable	0.50
h_{g1}/c	1.0	*Variable
h_{g2}/c	1.0	*Variable
α_1 (°)	70	70
α_2 (°)	70	70
w_g/w_r	1.0	1.0
P_B (N/m^2)	0.0	0.0
P_c (N/m^2)	−72139.79	−72139.79

Note*: – the geometrical and operating conditions of HGJBs used in cases 5 and 6.

Table III. Geometrical and operating conditions of HGJBs

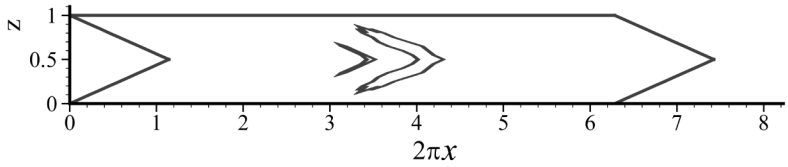

(a) Cavitation distribution for HGJBs for L_1:L_2=0.50:0.50 at ε =0.80

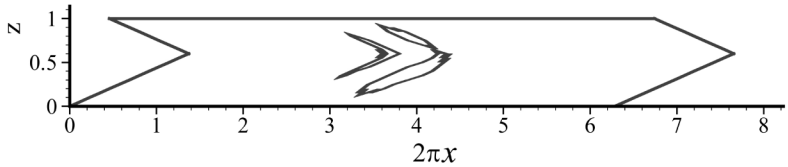

(b) Cavitation distribution for HGJBs for L_1:L_2=0.60:0.40 at ε =0.80

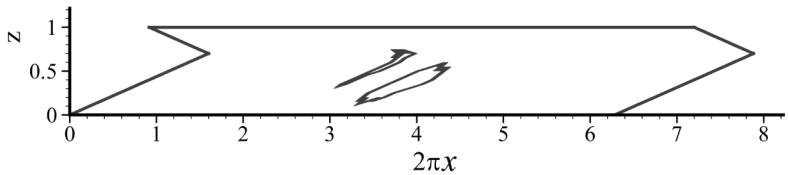

(c) Cavitation distribution for HGJBs for L_1:L_2=0.70:0.30 at ε =0.80

Figure 13.

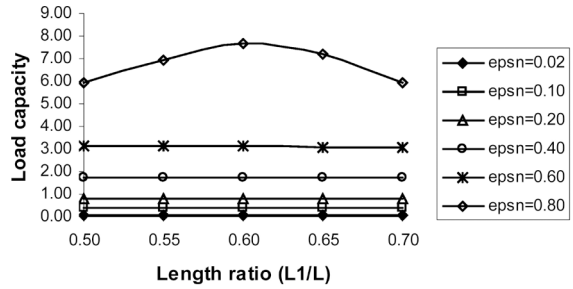

(a) Dimensionless load capacity due to the groove-length ratio

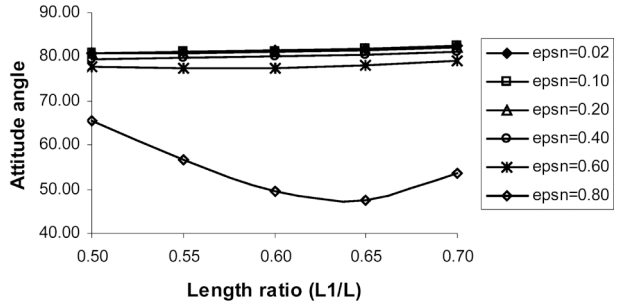

(b) Attitude angle due to the groove-length ratio

Figure 14.
The dimensionless load capacity (a) and attitude angle (b) due to the groove-length ratio and the eccentricity ratio (epsn)

For liquid-lubricated journal bearings, when the eccentricity ratio is not equal to zero, the fluid film is separated into two regions: the convergent region and the divergent region. In this case, the groove where $2\pi x = 0.9817$ (or $x = 0.15625$) in the x-axis (Figure 1) is located in the convergent region. Figures 11-13 show that, for non-symmetrical HGJBs, the pressure and cavitation distribution is asymmetrical, even the peak pressure is always reached at the apex of the herringbone grooves. When the groove-length ratio ($L_1 : L$) changes from 0.50 to 0.70, the cavitated region will be mainly located in part I of the fluid film, as shown in Figure 13.

5.1.2 The load capacity and attitude angle due to the groove-length ratio. Figure 14 shows the variance of dimensionless load capacity and attitude angle due to the variance of the groove-length ratio and the eccentricity ratio. This figure shows that, when the eccentricity ratio (ε or epsn in Figure 14) is not very large ($\varepsilon \leq 0.60$, for example in this case), the non-symmetrical HGJBs' dimensionless load capacity and attitude angle almost remain constant (at a constant eccentricity ratio), even though the groove-length ratio (L_1:L) changes from 0.50 to 0.70. It means that the influence of groove-length ratio on HGJBs' dimensionless load capacity and attitude angle can be ignored. On the other hand, when the eccentricity ratio increases to 0.80, the influence of groove-length ratio on HGJBs' dimensionless load capacity and attitude angle cannot be ignored.

5.1.3 Discussion. In this part, we studied the influence of the groove-length ratio on the performance of non-symmetrical HGJBs. The groove-length ratio ($L_1 : L$, varying from 0.50 to 0.70) and the eccentricity ratio (varying from 0.02 to 0.80) are considered. From the perspective of dimensionless load capacity and attitude angle, at a constant eccentricity ratio ($\varepsilon \leq 0.60$), the influence of groove-length ratio ($L_1 : L$) is very small (Figure 14). However, the pressure distribution shows that the influence of the groove-length ratio is very evident: at the same eccentricity ratio, along the groove, the peak pressure is always reached at the apex of the herringbone grooves (in the convergent region of the fluid film) when the groove-length ratio ($L_1 : L$) changes from 0.50 to 0.70, and when the eccentricity increases to some values, the cavitation will occur in the fluid film, thus, not only the pressure and cavitation distribution of the fluid film, but also the load capacity and attitude angle of HGJBs show that the influence of groove-length ratio cannot be ignored.

5.2 Effect of groove-depth ratio on non-symmetrical HGJBs

To study the effect of groove-depth ratio on the performance of non-symmetrical HGJBs, we assume that the depth of the grooves in part I is not equal to the depth of grooves in part II (Figure 1), even though in each part the groove depth is the same, respectively. We set $hg_1 : c = 1.0$ and change the value of $hg_2 : c$ from 0.2 to 1.0, thus $hg_2 : hg_1$ will vary from 0.2 to 1.0, while

other geometrical parameters of the two parts are the same (such as $L_1 = L_2$, $\alpha_1 = \alpha_2$ and so on). The numerical results are shown in Figures 15-18.

5.2.1 The pressure and cavitation distribution due to the groove-depth ratio. Figure 15 shows the pressure profiles along the grooves at $2\pi x = 0.9817$ (or $x = 0.15625$) in the fluid film. Just like what we have discussed earlier, in this case, the groove where $x = 0.15625$ in the x-axis is still located in the convergent region of the fluid film. Figures 16 and 17 show the pressure and cavitation distribution of the fluid film due to the variance of the groove-depth

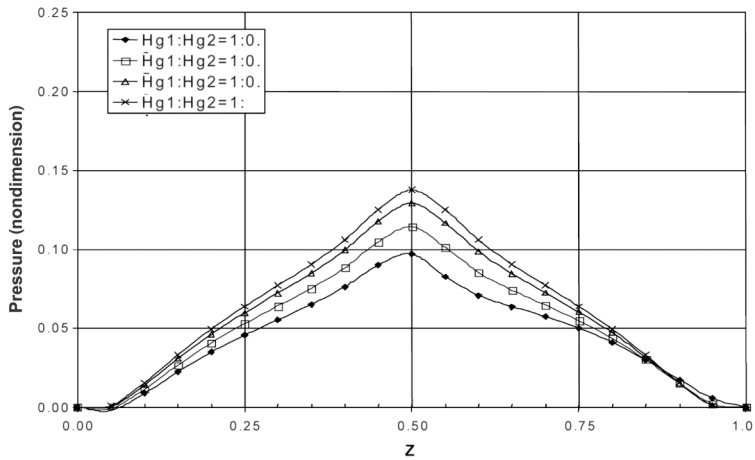

(a) Pressure distribution along grooves at $2\pi x = 0.9817$ for $\varepsilon = 0.02$

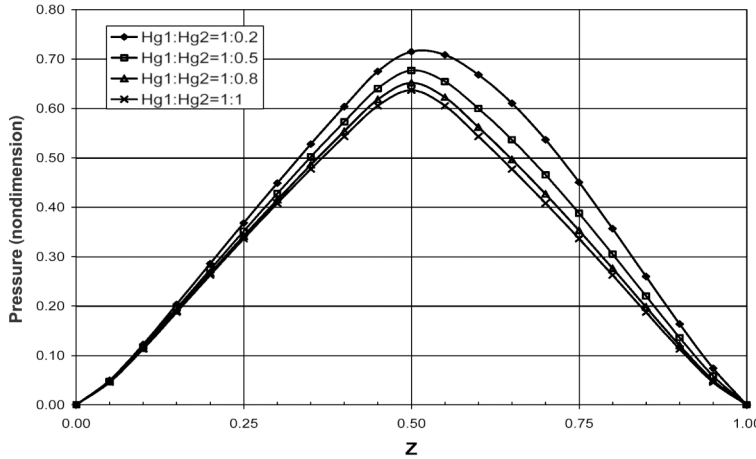

(b) Pressure distribution along grooves at $2\pi x = 0.9817$ for $\varepsilon = 0.40$

(continued)

Figure 15.

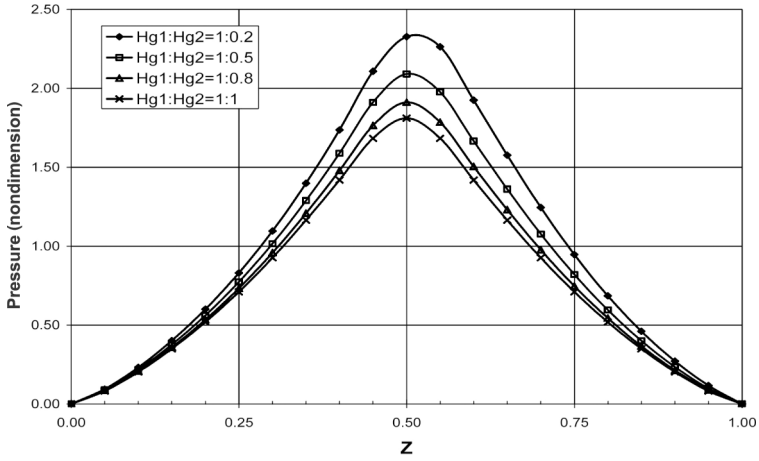

(c) Pressure distribution along grooves at $2\pi x = 0.9817$ for $\varepsilon = 0.80$

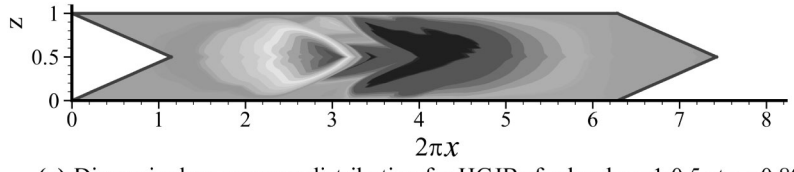

(a) Dimensionless pressure distribution for HGJBs for hg_1:hg_2=1:0.5 at ε =0.80

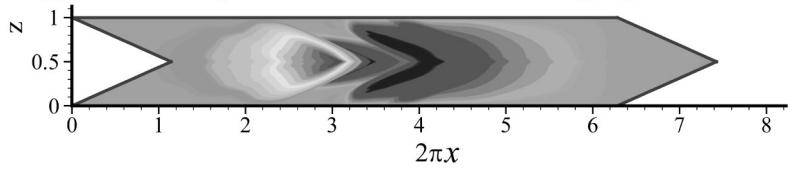

(b) Dimensionless pressure distribution for HGJBs for hg_1:hg_2=1:1 at ε =0.80

Figure 15.

Figure 16. Dimensionless pressure distribution due to the groove-depth ratio (h_{g1} : h_{g2}) for HGJBs (case 6 of Table III) at ε=0.80. (a) h_{g1} : h_{g2}=1:0.5; and (b) h_{g1} :h_{g2}=1 : 1

ratio ($hg_2 : hg_1 = 0.2 - 1$) under a constant eccentricity ratio ($\varepsilon = 0.80$). Figure 15 shows that the maximum pressure along the groove is always located at the apex of the herringbone groove. As shown in Figures 15-17, at a constant eccentricity ratio, when the groove-depth ratio is not equal to 1, the pressure and cavitation distribution is not symmetrical. Different groove's depth caused different pumping effect on the fluid. Hence, the pressure field and the cavitation distribution are different. The higher the groove-depth, the stronger is the groove's pumping effect.

5.2.2 The load capacity and attitude angle due to the groove-depth ratio. Figure 18 shows the dimensionless load capacity and the attitude angle's variance due to the groove-depth ratio and the eccentricity ratio. It shows that, at a constant groove-depth ratio, with the increase of the eccentricity ratio, the

dimensionless load capacity will also increase, while the attitude angle will decrease. On the other hand, because of the grooves' pumping effect to the fluid, at a constant eccentricity ratio, with the increase of the groove-depth ratio, the dimensionless load capacity will decrease. For attitude angle, only if the eccentricity ratio is not very large (for example, when $\varepsilon \leq 0.65$), then, at the same eccentricity ratio, with the increase of the groove-depth ratio, the attitude angle will decrease too. This is because that when the eccentricity ratio is not very large, there is no cavitation in the fluid film, then with the increase of the groove-depth ratio, the attitude angle will decrease. When the eccentricity ratio increases to some critical values, the cavitation will occur in the fluid film and the increase of the cavitated region will largely decrease the attitude angle. In other words, once the cavitation occurs in the fluid film, the influence of the cavitated region area on the attitude angle is much stronger than that of the groove-depth ratio. As shown in Figure 18(b), when $\varepsilon \geq 0.70$, with the increase of the groove-depth ratio (at the same eccentricity ratio), the attitude angle will also increase.

5.2.3 Discussion. In this part, we study the influence of the groove-depth ratio on the performance of non-symmetrical HGJBs. For this kind of non-symmetrical HGJBs, because the two parts have different groove depth, the grooves' pumping effect in the two parts are different from each other. Thus, the pressure and cavitation distribution is different between the two parts, even though the highest value of pressure is always located in the line of herringbone grooves' apexes. In terms of load capacity and attitude angle, at the same groove-depth ratio, with the increase of the eccentricity ratio, the dimensionless load capacity will increase, while the attitude angle will decrease (Figure 18). On the other hand, at a constant eccentricity ratio, the dimensionless load capacity decreases with the increase of the groove-depth ratio.

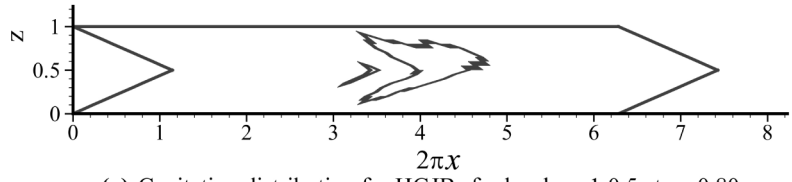

(a) Cavitation distribution for HGJBs for hg_1:hg_2=1:0.5 at ε =0.80

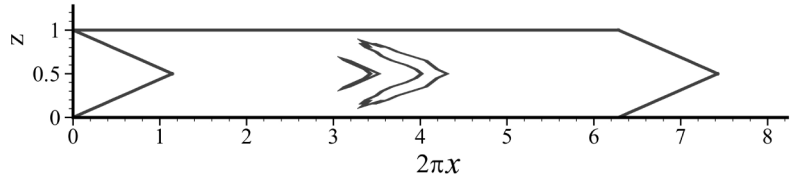

(b) Cavitation distribution for HGJBs for hg_1:hg_2=1:1 at ε =0.80

Figure 17.
Cavitation distribution due to the groove-depth ratio for HGJBs (case 6 of Table III) at $\varepsilon = 0.80$. (a) $h_{g1} : h_{g2}$=1:0.5; (b) $h_{g1} : h_{g2}$=1 : 1

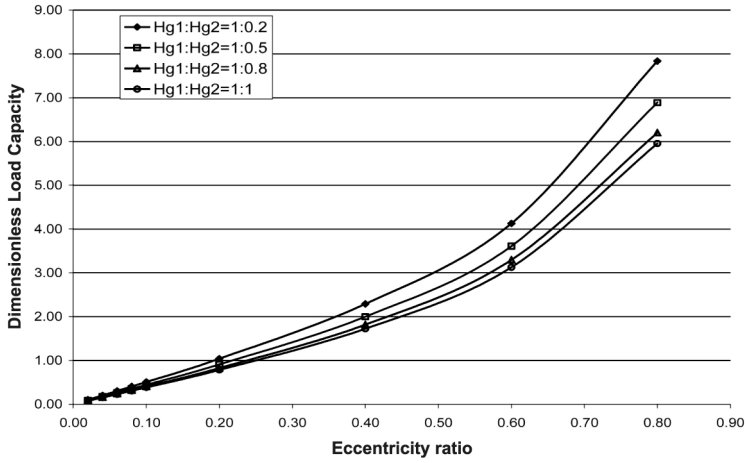

(a) Dimensionless load capacity due to groove-depth ratio

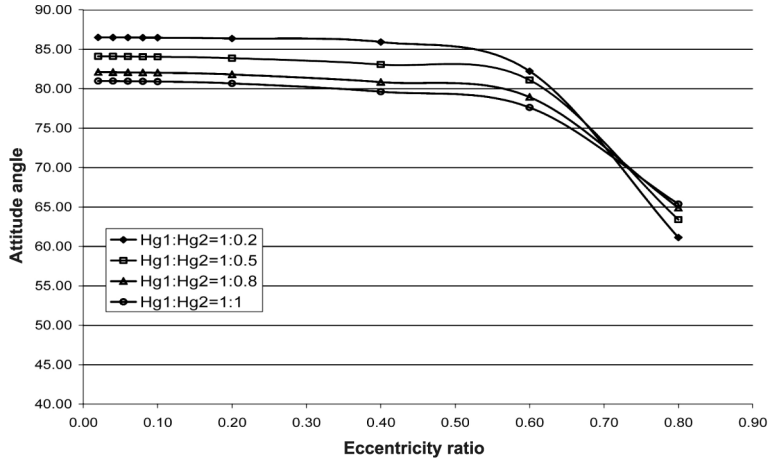

(b) Attitude angle due to the groove-depth ratio

Figure 18.

6. Conclusion

In this paper, first of all, a modified Elrod's algorithm is used to study the pumping effect of herringbone grooves: by engraving herringbone grooves on the surface of journal bearings, the cavitation region in fluid film is reduced obviously while comparing with the plain JBs (at the same eccentricity ratio). The journal bearing's stability is increased evidently: the HGJBs are free from one of the instable conditions – the half-frequency whirl. This is because of the herringbone grooves' pumping effect: the lubricant is pumped into the journal bearing along the grooves, thus the pressure is built up along the grooves.

When the HGJBs work at high rotating speed and low or non-eccentricity ratio, this kind of pressure will highly increase the shaft's self-centered ability, thus it will be more stable, compared with the plain JBs.

With the increase of the eccentricity ratio, the cavitation may occur in the fluid film of the HGJBs, both for plain JBs and for HGJBs. However, at the same eccentricity ratio, the cavitation ratio of the HGJB is much less than that of the plain JB. It is also found that, while working at the same eccentricity ratio, the HGJB's load capacity is less than that of the plain JB.

With the increase of the eccentricity ratio, the dimensionless load capacity will also increase, while the attitude angle will decrease. It is the same for all kinds of journal bearings studied here. However, the variation of the dimensionless load capacity and the attitude angle due to the eccentricity ratio is different for plain journal bearings, symmetrical and non-symmetrical HGJBs.

For the non-symmetrical HGJBs, the effect of the groove-length ratio and the groove-depth ratio on the HGJBs' performance is investigated. It is found that, for the asymmetrical groove patterns, the pressure and cavitation distribution within the fluid film of the journal bearing is asymmetrical. The influence of the groove-length ratio or the groove-depth ratio on the herringbone grooves' pumping effect is very evident.

References

Brewe, D.E. (1986), "Theoretical modeling of the vapor cavitation in dynamically loaded journal bearings", *ASME Journal of Tribology*, Vol. 108, pp. 628-38.

Dowson, D. and Taylor, C.M. (1979), "Cavitation in bearings", *Annual Review of Fluid Mechanics*, pp. 35-66.

Elrod, H.G. (1981), "A cavation algorithm", *ASME Journal of Lubrication Technology*, Vol. 103 No. 3, pp. 350-4.

Elrod, H.G. and Adams, M.L. (1974), "A computer program for cavitation and starvation problems", in, *Cavitation and Related Phenomena in Lubrication*, Mechanical Engineering Publications, New York, NY, pp. 37-41.

Fuller, D.D. (1984), *Theory and Practice of Lubrication for Engineers*, 2nd ed., Wiley, New York, NY, pp. 362-85.

Hagg, A.C. (1946), "The influence of oil-film journal bearings on the stability of rotating machines", *ASME Trans. J. Appl. Mech.*, Vol. 68, pp. A211-20.

Hirs, G.G. (1965), "The load capacity and stability characteristics of hydrodynamic grooved journal bearings", *ASLE Transactions*, Vol. 8, pp. 296-305.

Jakobsson, B. and Floberg, L. (1957), "The finite journal bearing considering vaporization", *Transactions of Chalmers University of Technology*, Guthenburg, Sweden, p. 190.

Jang, G.H. and Chang, D.I. (2000), "Analysis of hydrodynamic herringbone grooved journal bearing considering cavitation", *ASME Journal of Tribology*, Vol. 122, pp. 103-9.

Olsson, K.O. (1965), "Cavation in dynamically loaded bearing", *Transactions of Chalmers University of Technology*, Guthenburg, Sweden, p. 308.

Shu, C., Chen, W. and Du, H. (2000), "Free vibration analysis of curvilinear quadrilateral plates by differential quadrature method", *J. Comput. Phys.*, Vol. 163 No. 2, pp. 452-66.

Vijayaraghavan, D. and Keith, T.G. Jr (1990a), "An efficient, robust and time accurate numerical procedure applied to a cavitation algorithm", *ASME Journal of Tribology*, Vol. 112, pp. 44-51.

Vijayaraghavan, D. and Keith, T.G. Jr (1990b), "Grid transformation and adaption techniques applied to the analysis of cavitated journal bearings", *ASME Journal of Tribology*, Vol. 112, pp. 52-9.

Wan, J.M., Lee, T.S., Shu, C. and Wu, J. (2002), "A numerical study of cavitation foot-prints in liquid-lubricated non-symmetrical herringbone grooved journal bearings", *International Journal of Numerical Methods for Heat and Fluid Flow*, Paper No. HFF671.